Lithium Ion Pathway within Li₇La₃Zr₂O₁₂-Polyethylene Oxide Composite Electrolytes

Jin Zheng[+], Mingxue Tang[+], and Yan-Yan Hu*

Abstract: *Polymer–ceramic composite electrolytes are emerging as a promising solution to deliver high ionic conductivity, optimal mechanical properties, and good safety for developing high-performance all-solid-state rechargeable batteries. Composite electrolytes have been prepared with cubic-phase $Li_7La_3Zr_2O_{12}$ (LLZO) garnet and polyethylene oxide (PEO) and employed in symmetric lithium battery cells. By combining selective isotope labeling and high-resolution solid-state Li NMR, we are able to track Li ion pathways within LLZO-PEO composite electrolytes by monitoring the replacement of ^7Li in the composite electrolyte by ^6Li from the ^6Li metal electrodes during battery cycling. We have provided the first experimental evidence to show that Li ions favor the pathway through the LLZO ceramic phase instead of the PEO-LLZO interface or PEO. This approach can be widely applied to study ion pathways in ionic conductors and to provide useful insights for developing composite materials for energy storage and harvesting.*

$\mathbf{R}$echargeable lithium ion batteries (LIBs) are one of the leading technologies for energy storage.[1,2] Developing suitable electrolytes for high-voltage, high-energy-density, and safe LIBs is important yet challenging.[3,4] Electrolytes commonly employed in LIBs are dissolved in organic solvents, which are flammable and often decompose at high voltages. In addition, Li dendrite growth across liquid-based electrolytes causes safety issues and limits the utilization of Li metal as anodes.[5–7] To overcome these challenges, non-flammable solid-state electrolytes are suitable alternatives to organic-solvent-based electrolytes.[8–14] Inorganic ceramics and organic polymers are two general classes of materials used as solid electrolytes for LIBs. Among all inorganic ceramics, garnet-type electrolytes show very high ionic conductivity and chemical stability. For instance, cubic-phase $Li_7La_3Zr_2O_{12}$ (LLZO) exhibited an ionic conductivity of $\sigma_{bulk} \approx 10^{-4}$ S cm at room temperature with superior stability[15] and a wide electrochemical voltage window.[16–18] How-

ever, ceramic materials are often too rigid and brittle, and show poor contact with electrodes.[19,20] Flexible polymer electrolytes exhibit more suitable mechanical properties than ceramics, but show low ionic conductivity at room temperature and poor stability at high temperatures.[21,22] Polyethylene oxide (PEO)-based materials are widely considered as promising candidates for LIBs because of their compatibility with lithium salts and low cost.[23,24] The combination of ceramics and polymers offers a new path to create better electrolytes with both high ionic conductivity and good mechanical properties.

Ionic conductivity of composite electrolytes is critical to their applications in all-solid-state rechargeable batteries. The ratio and integration of polymer and ceramics in composite electrolytes strongly affect their properties and performance. Significant improvement in the ionic conductivity of polymer electrolytes was obtained with the addition of ceramic particles.[25–27] It was suggested that an amorphous polymer shell formed around filler particles accounts for the increase in ionic conductivity.[9,28–30] Finite element simulations also revealed[28–30] that ion conduction within composite electrolytes mainly occurs at the ceramic–polymer interface. However, other hypotheses suggested that Li ions diffuse through the ceramic particles.[20,31] Experimental evidence is needed to resolve the debate surrounding Li ion pathways in composite materials.

As a very light element, Li is difficult to characterize with electron- or X-ray-based techniques. The polymer–ceramic composite electrolyte adds another layer of complexity for tracking Li ion diffusion. Li nuclear magnetic resonance (NMR) has proven to be a powerful tool to study local structural environments and dynamics of Li ions.[32–38] To this end, we first apply high-resolution solid-state Li NMR to determine the local structural environments of Li ions in the PEO polymer, the LLZO ceramic phase, and at the LLZO-PEO interface. Both ^{7}Li and ^{6}Li are NMR active isotopes, which allow a unique way for probing Li ion transport pathways within composite electrolytes using isotope exchange. To determine possible lithium ion pathways, a symmetric battery made with ^{6}Li-labeled lithium foils sandwiching a LLZO-PEO (LiClO₄) composite electrolyte film was electrochemically cycled. In this symmetric battery, ^{6}Li ions were stripped from one ^{6}Li electrode into the electrolyte by electric potential, and then diffused through the electrolyte to deposit onto the other ^{6}Li electrode. Meanwhile, ^{6}Li ions partially replace ^{7}Li ions inside the electrolyte every time they move through the electrolyte, leaving a trail for the Li ion pathway. By comparing ^{6}Li and ^{7}Li NMR of pristine and cycled composite electrolytes, we are able to reveal Li ion pathways within the composite electrolyte.

[*] Prof. Y.-Y. Hu
Center of Interdisciplinary Magnetic Resonance
National High Magnetic Field Laboratory
1800 East Paul Dirac Drive, Tallahassee, FL 32310 (USA)
E-mail: hu@chem.fsu.edu

J. Zheng,[+] Dr. M. Tang,[+] Prof. Y.-Y. Hu
Department of Chemistry and Biochemistry
Florida State University
Tallahassee, FL 32306 (USA)

[+] These authors contributed equally to this work.

Supporting information and the ORCID identification number(s) for the author(s) of this article can be found under http://dx.doi.org/10.1002/anie.201607539.

The composite electrolyte was prepared using PEO (LiClO$_4$) and LLZO (Figure 1 a), which were ball-milled and dried in vacuum. The procedure for making the composite electrolyte is depicted in Figure 1. Symmetric lithium batteries were assembled with as-prepared composite electrolytes and ^{6}Li metal foils.
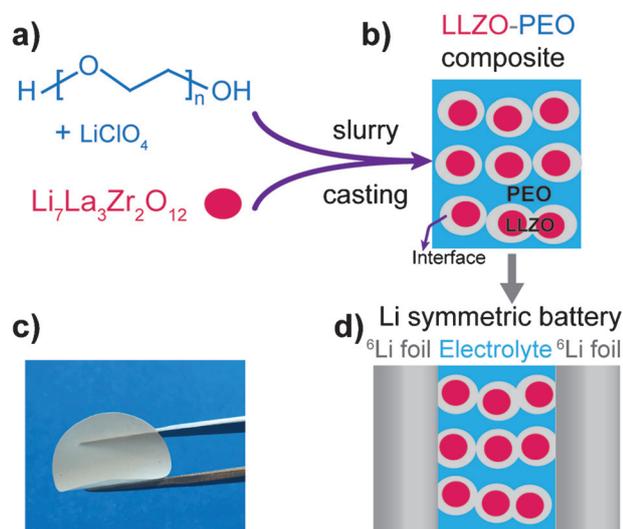

Figure 1. a,b) Illustration of the process for preparing LLZO-PEO composite electrolytes. c) Picture of the as-synthesized flexible composite electrolyte. d) Schematic of a symmetric battery made of ^{6}Li foil/composite electrolyte/^{6}Li foil for probing Li ion pathways within the composite electrolyte. In the illustration, the blue area represents the PEO polymer matrix, red filled circles are LLZO particles, and the white regions represent the interface between PEO and LLZO.

Figure 2. a) Diagram of local Li environments in LLZO-PEO (LiClO$_4$) composites. b) ^{6}Li NMR of LiClO$_4$ in PEO, pure cubic-LLZO, and LLZO-PEO (LiClO$_4$) composite. c) ^{6}Li direct polarization (DP) and d) ^{6}Li cross polarization (CP) NMR spectra, spectral simulation, assignments, and quantification results for the LLZO-PEO (LiClO$_4$) composite.

NMR is sensitive to local structural environments and therefore can be used to distinguish Li ions in the polymer phase, the ceramic phase, and at the polymer–ceramic interface within composite electrolytes. For this purpose, ^{6}Li NMR is preferred for its much higher resolution compared to ^{7}Li NMR because strong ^{7}Li–^{7}Li dipolar interactions significantly broaden ^{7}Li resonances and result in overlapped peaks in ^{7}Li NMR. ^{7}Li NMR was employed for spin exchange experiments, which take advantage of strong ^{7}Li–^{7}Li dipolar interactions.

Possible Li local environments within the LLZO-PEO (LiClO$_4$) composite electrolyte are depicted in Figure 2 a. High-resolution ^{6}Li NMR spectra of LLZO-PEO (LiClO$_4$) composites are shown in Figure 2 b–d. The ^{6}Li NMR spectra of pure LLZO and LiClO$_4$ in PEO polymer (Figure 2 b) were used as references. A single ^{6}Li resonance at −0.2 ppm was observed for LiClO$_4$ within the PEO polymer matrix and at 2 ppm for Li in pure cubic-LLZO (Figure 2 b, bottom). In the ^{6}Li spectrum of the LLZO-PEO (LiClO$_4$) composite, in addition to the −0.2 ppm and 2.0 ppm peaks, a third component at around 1.4 ppm (shown as a broad shoulder of the LLZO peak) was assigned to Li at the PEO and LLZO interface. Detailed assignments, spectral simulations, and quantifications are given in Figure 2 c and d. Quantification
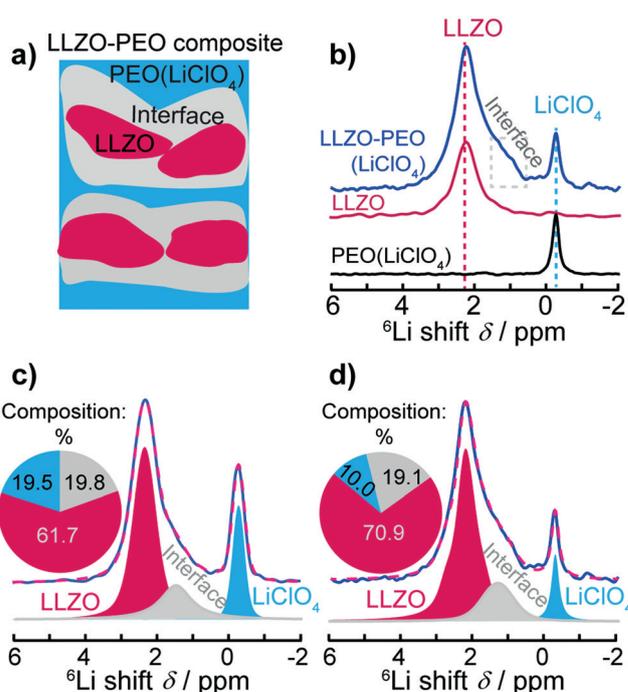
results obtained from the ^{6}Li spectrum of the LLZO-PEO (LiClO$_4$) composite recorded using direct polarization (DP, Figure 2 c) showed 10.0 mol % Li in the PEO phase, 70.9 mol % Li in LLZO, and 19.1 mol % Li at the interface. ^{6}Li cross polarization (CP) NMR was obtained by polarizing ^{1}H spins in the PEO phase first, followed by transferring ^{1}H polarization to ^{6}Li over a time period of 6 ms (CP contact time). In general, a longer CP contact time allows for greater polarization transfer from ^{1}H to ^{6}Li. The CP process is driven by dipolar coupling interactions between ^{1}H and ^{6}Li spins, which strongly depend on the ^{1}H–^{6}Li distance. Therefore, the LiClO$_4$ (in PEO) signal is preferentially enhanced (19.5 mol %) due to a shorter average LiClO$_4$–PEO distance, Li in LLZO is underrepresented due to a longer ^{1}H PEO–LLZO distance, and the interfacial ^{7}Li stays more or less the same (19.1 mol %) in the ^{6}Li CP spectrum (Figure 2 d). This confirmed the assignment of interfacial Li in the ^{6}Li spectra of LLZO–PEO (LiClO$_4$) composites.

Further confirmation for the assignment of interfacial Li in ^{6}Li spectra of LLZO-PEO (LiClO$_4$) composites was obtained from the CP build-up rate (Figure 3) and spin exchange process (Figure 4). The ^{6}Li CP NMR spectra at different contact times are shown in Figure 3 a. All of the Li components increased in intensity as contact time increased from 0.1 to 6.0 ms. The intensity increase of the LiClO$_4$ resonance (in the PEO phase), LLZO, and interfacial Li as a function of contact time was plotted individually and shown in Figure 3 b. The interfacial Li shows faster build-up than Li in the LLZO. As mentioned above, the CP process is strongly
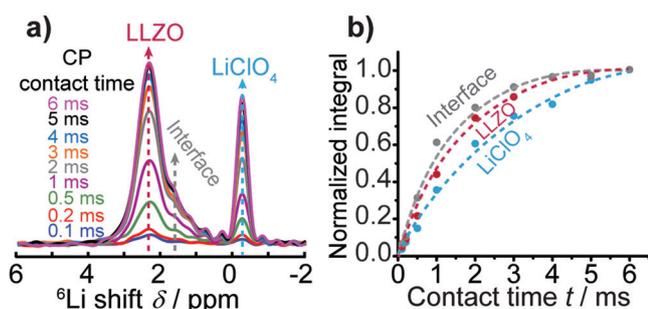
Figure 3. a) $^1H-^6Li$ CP spectra as a function of contact times for pristine LLZO-PEO ($LiClO_4$) electrolyte, contact times are listed to the left of the spectra and the dashed arrows indicate the direction of increasing contact times. b) CP build-up plots for interfacial Li, Li in LLZO, and Li from $LiClO_4$ inside the PEO phase.
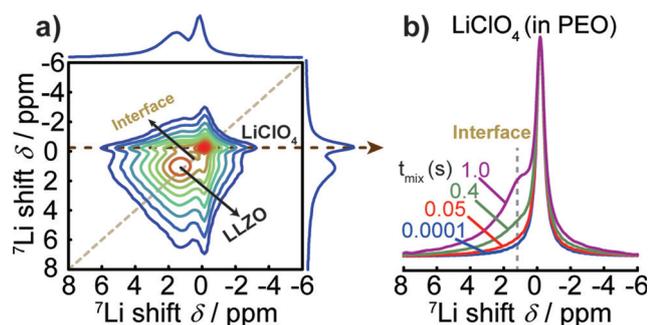

Figure 4. a) ^7Li 2D EXSY spectrum of pristine LLZO-PEO ($LiClO_4$) composite electrolytes, and b) cross-section taken from the 2D EXSY spectrum of the PEO($LiClO_4$) peak at the position indicated by the arrowhead dashed line, with mixing times of 0.0001, 0.05, 0.4, and 1.0 s.

distance-dependent. Therefore, this confirmed that the assigned interfacial Li is closer to the PEO phase than Li in the LLZO. In principle, the $LiClO_4$ signal should reach the maximum first due to the shortest distance to ^1H within PEO. However, the result shows a relatively slow buildup for the $LiClO_4$ component (Figure 3b), likely owing to the fast tumbling motion of small Li ions in $LiClO_4$ which weakens the $^1H-^6Li$ dipolar coupling and makes the CP process less efficient. $^1H-^6Li$ CP NMR on cycled LLZO-PEO electrolytes (Figures S1 and S2) also confirmed the assignment of interfacial Li resonances.

The relative spatial disposition of different Li components can also be probed with ^7Li 2D exchange spectroscopy (EXSY).[39] A cross peak in a 2D EXSY spectrum at frequency coordinates (δA, δB) indicates in general that the spin resonating at δA is interacting with, and thus spatially close to, the spin resonating at δB. Figure 4a shows an example of ^7Li 2D-EXSY spectra for pristine LLZO-PEO ($LiClO_4$) composites. In the contour plot (Figure 4a), the two circle regions located on the diagonal are peaks from LLZO and $LiClO_4$ inside PEO, respectively. The region between LLZO and $LiClO_4$ peaks on the diagonal in the 2D EXSY spectrum is from interfacial Li. In 2D EXSY experiments, a mixing time period is set to allow spin interactions among LLZO, $LiClO_4$, and interfacial Li. Longer mixing times often

permit spin interactions over a larger spatial range. If spin interactions occur, off-diagonal peaks (also known as cross peaks) will show in the 2D EXSY spectra that connect the two interactive components. To more clearly observe the spin exchange process, 1D cross sections were taken at the chemical shift of $LiClO_4$ from the 2D EXSY spectra (as indicated by the horizontal dashed line) with mixing times of 0.0001, 0.05, 0.4, and 1.0 s. These 1D cross-section spectra (in Figure 4b) reveal all of the other components that interact with $LiClO_4$ due to spatial vicinity. At a very short mixing time of 0.1 ms, only the $LiClO_4$ peak was observed (blue). Upon gradual increase of the mixing time up to 1.0 s, the ^6Li peak at 1.4 ppm from the interfacial Li grew stronger, suggesting spin exchange between $LiClO_4$ in PEO and interfacial Li. No spin exchange between $LiClO_4$ and LLZO was observed owing to their relatively large distance apart. In summary, the 2D ^7Li EXSY experiments of LLZO-PEO composites confirm the ^6Li resonance assignment of interfacial Li at 1.4 ppm.

So far, a clear assignment of Li in the PEO phase, Li in LLZO, and interfacial Li has been made and confirmed. The interfacial Li resonance is significantly broader than LLZO and $LiClO_4$ in PEO, indicating a larger degree of structural disorder at the interface. The ^6Li NMR chemical shift of interfacial Li (1.4 ppm) is very close to that of Li from LLZO (2.0 ppm), which suggests that interfacial Li is from the LLZO surface and is heavily affected by PEO matrix.

To probe Li^+ ion pathways within the LLZO-PEO ($LiClO_4$) composite electrolyte during battery cycling, a symmetric battery was assembled with LLZO-PEO ($LiClO_4$) electrolyte and ^6Li metal electrodes (Figure 5a). The symmetric cell was cycled using a constant current density of 61 $\mu A\,cm^{-2}$ and a slightly biased potential that changed sign every 5 min. Upon battery cycling, ^6Li ions move from one electrode, across the composite electrolyte, to the other electrode. On their way, ^6Li ions replace ^7Li ions in the LLZO-PEO ($LiClO_4$) composite electrolyte, leaving a trail of the diffusion pathway. By comparing the ^6Li spectra of the composite electrolyte before and after electrochemical cycling, an increase in the ^6Li peak intensity can be observed for those Li local environments where ^6Li ions pass. As shown in Figure 5c, the ^6Li spectrum of the cycled composite electrolyte showed significantly increased intensity for the LLZO peak, and only a slight increase for the interfacial Li and $LiClO_4$ resonances compared with that of the pristine LLZO-PEO ($LiClO_4$) composite. This indicates that a large amount of ^6Li replaced ^7Li within LLZO. The replacement could be further quantified based on spectral simulation (Figure 5d). The peak intensity of LLZO increased by 39%, only a 6% increment was found for interfacial Li, and there was very little or no increase for $LiClO_4$ in PEO. Complementary ^7Li spectra of pristine and cycled LLZO-PEO ($LiClO_4$) composite electrolytes show decreased intensity of ^7Li LLZO resonance, confirming the replacement of ^7Li by passing ^6Li ions in the LLZO phase (Figure S3). Additionally, a ^7Li foil/composite electrolyte/^7Li foil symmetric battery was assembled and cycled under the same condition as for the ^6Li symmetric cell. A slightly increased ^7Li signal was only observed for the LLZO peak after cycling (Figure S3); this is
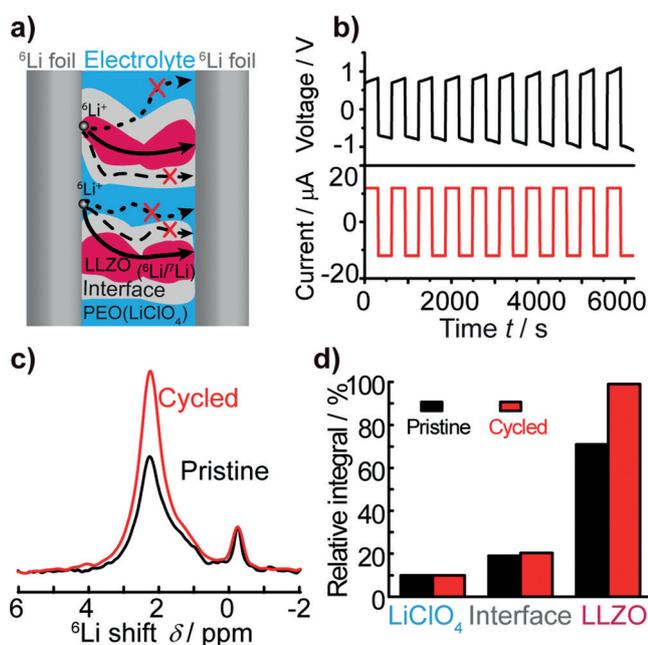
Figure 5. a) Illustration of the symmetric ^{6}Li foil/composite electrolyte/^{6}Li foil battery and possible Li$^+$ transport pathways within the composite electrolyte upon cycling the symmetric battery. b) Electrochemical profile of the symmetric lithium battery cycled with a constant current that changes signs every 300 s. c) Comparison of the ^{6}Li NMR spectra of the LLZO-PEO (LiClO$_4$) composite electrolytes before (pristine) and after (cycled) cycling. d) Quantitative analysis of ^{6}Li amount in LiClO$_4$, interface, and LLZO of the LLZO-PEO (LiClO$_4$) before and after cycling.

because ^{7}Li ions replace ^{6}Li (7.6 atom % natural abundance) on their way through the electrolyte. The results obtained from the ^{7}Li symmetric cell further confirmed that Li ions diffuse through LLZO particles, consistent with the investigation using the ^{6}Li symmetric cell. Possible Li ion pathways are indicated in Figure 5a. In summary, the ^{6,7}Li NMR results show that Li ions prefer to go through LLZO particles and minimize the fraction of polymer phase or interface on their pathway when possible. LLZO accounts for about 20 vol % in the composite electrolytes; in order to allow Li ion transport to largely occur in the LLZO phase, LLZO particles need to form a percolation network.

In conclusion, various Li local structural environments within LLZO-PEO (LiClO$_4$) composite electrolytes have been resolved by 1D high-resolution ^{6}Li NMR. ^{6}Li CP and ^{7}Li 2D EXSY NMR confirmed the assignment of NMR resonance for interfacial Li. The replacement of ^{7}Li by ^{6}Li ions in the LLZO ceramic phase of the LLZO-PEO (LiClO$_4$) composite electrolyte, when used in a symmetric (^{6}Li electrode/composite electrolyte/^{6}Li electrode) battery cell, indicates that Li ions prefer to maximize the fraction of the LLZO ceramic phase and minimize that of the interface or the PEO polymer phase on their diffusion pathway. We have succeeded in employing Li NMR to probe Li ion diffusion pathway within LLZO-PEO (LiClO$_4$) composite electrolytes employed in all-solid-state batteries. Our study provides the first experimental evidence to show that Li ions mainly pass through LLZO ceramic particles, not the interface or the

PEO polymer phase. The method used here, that is, using NMR active isotopes of the same element to track ion diffusion pathway, can be widely applied in materials and chemistry research.

Experimental Section

Cubic LLZO (Li$_7$La$_3$Zr$_2$O$_{12}$) garnet was synthesized with solid-state reactions using 19.8 wt % LiOH (Sigma–Aldrich, ≥ 98 %; pre-dried at 200 °C for 6 h; 52.5 wt % La$_2$O$_3$ (Sigma–Aldrich, ≥ 99.9 %; pre-dried at 900 °C for 12 h), 26.5 wt % ZrO$_2$ (Sigma–Aldrich, ≥ 99 %), and 1.2 wt % Al$_2$O$_3$. The mixed powder was ball-milled for 0.5 h using a SPEX SamplePrep 8000M mixer/mill. The mixture was then calcined at 800 °C for 12 h. After cooling down, the powder was reground and pressed into a pellet, which was sintered at 1000 °C for 36 h and crushed into powder again by ball–milling for 1 h.

The composite electrolyte was prepared with a solution-casting method. PEO (Sigma–Aldrich, MW = 400 000) and LiClO$_4$ (Sigma–Aldrich, ≥ 99.99 %; vacuum dried at 100 °C for 24 h) were dissolved in anhydrous acetonitrile by stirring at 80 °C for 12 h in an argon-filled glovebox. The [EO]/[Li] ratio was fixed at 18:1, and the amount of LLZO powder added was 50 wt %, corresponding to 20 vol %. The PEO/LiClO$_4$/acetonitrile solution and LLZO powder were mixed by ball-milling for 1 h. The homogeneous slurry was cast on a flat Teflon plate using a doctor blade. The film was dried in vacuum at 50 °C for 12 h. The thickness of the composite electrolyte ranged from 30 µm to 50 µm.

The symmetric battery cell was assembled by pressing Li foils on both sides of the composite electrolyte film. Charge and discharge cycling of the symmetric cell was conducted at a constant current density of 61 µA cm^{-2} on a LANHE battery testing system.

Solid-state NMR spectra were acquired on a Bruker Avance III-500 at Larmor frequencies of 73.6 and 194.4 MHz for ^{6}Li and ^{7}Li, respectively. A 2.5 mm Bruker HXY probe was used and the samples were spun at 25 kHz for DP and 10 kHz for CP. The ^{6,7}Li chemical shift was referenced to solid LiCl at 0 ppm.

[1] M. Armand, J.-M. Tarascon, *Nature* **2008**, *451*, 652–657.
[2] P. G. Bruce, B. Scrosati, J.-M. Tarascon, *Angew. Chem. Int. Ed.* **2008**, *47*, 2930–2946; *Angew. Chem.* **2008**, *120*, 2972–2989.
[3] J.-M. Tarascon, M. Armand, *Nature* **2001**, *414*, 359–367.
[4] V. Etacheri, R. Marom, R. Elazari, G. Salitra, D. Aurbach, *Energy Environ. Sci.* **2011**, *4*, 3243.
[5] K. Xu, *Chem. Rev.* **2004**, *104*, 4303–4418.
[6] K. Tasaki, *J. Phys. Chem. B* **2005**, *109*, 2920–2933.
[7] K. Xu, *Chem. Rev.* **2014**, *114*, 11503–11618.
[8] F. Croce, G. B. Appetecchi, L. Persi, B. Scrosati, *Nature* **1998**, *394*, 456–458.
[9] Z. Gadjourova, Y. G. Andreev, D. P. Tunstall, P. G. Bruce, *Nature* **2001**, *412*, 520–523.

[10] S. Stramare, V. Thangadurai, W. Weppner, *Chem. Mater.* **2003**, *15*, 3974–3990.

[11] J. Hassoun, B. Scrosati, *Angew. Chem. Int. Ed.* **2010**, *49*, 2371–2374; *Angew. Chem.* **2010**, *122*, 2421–2424.

[12] M. Balaish, E. Peled, D. Golodnitsky, Y. Ein-Eli, *Angew. Chem. Int. Ed.* **2015**, *54*, 436–440; *Angew. Chem.* **2015**, *127*, 446–450.

[13] I. Osada, H. de Vries, B. Scrosati, S. Passerini, *Angew. Chem. Int. Ed.* **2016**, *55*, 500–513; *Angew. Chem.* **2016**, *128*, 510–523.

[14] M. R. Busche, T. Drossel, T. Leichtweiss, D. A. Weber, M. Falk, M. Schneider, M.-L. Reich, H. Sommer, P. Adelhelm, J. Janek, *Nat. Chem.* **2016**, *8*, 426–434.

[15] R. Murugan, V. Thangadurai, W. Weppner, *Angew. Chem. Int. Ed.* **2007**, *46*, 7778–7781; *Angew. Chem.* **2007**, *119*, 7925–7928.

[16] S. Ohta, T. Kobayashi, J. Seki, T. Asaoka, *J. Power Sources* **2012**, *202*, 332–335.

[17] K. Ishiguro, Y. Nakata, M. Matsui, I. Uechi, Y. Takeda, O. Yamamoto, N. Imanishi, *J. Electrochem. Soc.* **2013**, *160*, A1690–A1693.

[18] W. Xia, B. Xu, H. Duan, Y. Guo, H. Kang, H. Li, H. Liu, *ACS Appl. Mater. Interfaces* **2016**, *8*, 5335–5342.

[19] Y. Inda, T. Katoh, M. Baba, *J. Power Sources* **2007**, *174*, 741–744.

[20] N. M. Asl, J. Keith, C. Lim, L. Zhu, Y. Kim, *Electrochim. Acta* **2012**, *79*, 8–16.

[21] H. M. J. C. Pitawala, M. A. K. L. Dissanayake, V. A. Seneviratne, *Solid State Ionics* **2007**, *178*, 885–888.

[22] J. Syzdek, M. Armand, M. Marcinek, A. Zalewska, G. Żukowska, W. Wieczorek, *Electrochim. Acta* **2010**, *55*, 1314–1322.

[23] Z. Xue, D. He, X. Xie, *J. Mater. Chem. A* **2015**, *3*, 19218–19253.

[24] W. H. Meyer, *Adv. Mater.* **1998**, *10*, 439–448.

[25] Y.-C. Jung, S.-K. Kim, M.-S. Kim, J.-H. Lee, M.-S. Han, D.-H. Kim, W.-C. Shin, M. Ue, D.-W. Kim, *J. Power Sources* **2015**, *293*, 675–683.

[26] J.-H. Choi, C.-H. Lee, J.-H. Yu, C.-H. Doh, S.-M. Lee, *J. Power Sources* **2015**, *274*, 458–463.

[27] W. Liu, N. Liu, J. Sun, P.-C. Hsu, Y. Li, H.-W. Lee, Y. Cui, *Nano Lett.* **2015**, *15*, 2740–2745.

[28] W. E. Tenhaeff, X. Yu, K. Hong, K. A. Perry, N. J. Dudney, *J. Electrochem. Soc.* **2011**, *158*, A1143–A1149.

[29] S. Kalnaus, A. S. Sabau, W. E. Tenhaeff, N. J. Dudney, C. Daniel, *J. Power Sources* **2012**, *201*, 280–287.

[30] S. Kalnaus, W. E. Tenhaeff, J. Sakamoto, A. S. Sabau, C. Daniel, N. J. Dudney, *J. Power Sources* **2013**, *241*, 178–185.

[31] S. S. Lee, Y. J. Lim, H. W. Kim, J.-K. Kim, Y.-G. Jung, Y. Kim, *Solid State Ionics* **2016**, *284*, 20–24.

[32] C. P. Grey, N. Dupré, *Chem. Rev.* **2004**, *104*, 4493–4512.

[33] R. Bhattacharyya, B. Key, H. Chen, A. S. Best, A. F. Hollenkamp, C. P. Grey, *Nat. Mater.* **2010**, *9*, 504–510.

[34] F. Blanc, M. Leskes, C. P. Grey, *Acc. Chem. Res.* **2013**, *46*, 1952–1963.

[35] Y.-Y. Hu, Z. Liu, K.-W. Nam, O. J. Borkiewicz, J. Cheng, X. Hua, M. T. Dunstan, X. Yu, K. M. Wiaderek, L.-S. Du et al., *Nat. Mater.* **2013**, *12*, 1130–1136.

[36] A. J. Ilott, N. M. Trease, C. P. Grey, A. Jerschow, *Nat. Commun.* **2014**, *5*, 4536.

[37] L.-Y. Yang, D.-X. Wei, M. Xu, Y.-F. Yao, Q. Chen, *Angew. Chem. Int. Ed.* **2014**, *53*, 3631–3635; *Angew. Chem.* **2014**, *126*, 3705–3709.

[38] L. Zhou, M. Leskes, T. Liu, C. P. Grey, *Angew. Chem. Int. Ed.* **2015**, *54*, 14782–14786; *Angew. Chem.* **2015**, *127*, 14995–14999.

[39] A. D. Bain, *Prog. Nucl. Magn. Reson. Spectrosc.* **2003**, *43*, 63–103.